MM Science Journal | www.mmscience.eu
ISSN 1803-1269 (Print) | ISSN 1805-0476 (On-line)
Special Issue | TEAM 2024
Transdisciplinary and Emerging Approaches to Multidisciplinary Science
11.9.2024 – 13.9.2024, Ostrava, Czech Republic
DOI: 10.17973/MMSJ.2024_12_2024126

TEAM2024-00039

SURFACE INVESTIGATION OF HIGH TEMPERATURE WEAR BEHAVIOR OF SS316L ALLOY PRODUCED BY LASER POWDER BED FUSION

Navin Kumar[1*], Palanisamy Chandrakumar[1], Arun Prasad Murali[1], Preeti Gautam[2], Petr Nemecek[2], Michal Prusa[2]

1Department of Mechanical Engineering, Vel Tech Rangarajan Dr. Sagunthala R&D Institute of Science and Technology, Chennai 600062, India; kumarnavin31794@gmail.com;

2Department of Machining, Assembly and Engineering Metrology, Faculty of Mechanical Engineering, VSB-Technical University of Ostrava, 70800 Ostrava, Czech Republic; preeti.gautam@vsb.cz;

*Corresponding author: kumarnavin31794@gmail.com

Abstract
This research investigates the tribological characteristics of SS316L produced through Laser Powder Bed Fusion (LPBF), emphasizing the influence of testing temperature, sliding velocity, and loading conditions. The findings demonstrate that the friction coefficient escalates with increased temperatures (150°C and 250°C), whereas the wear rate remains invariant, presumably attributable to the establishment of a lubricating surface layer. The rotational velocity of 300 revolutions per minute the Coefficient of Friction (COF) shown an upward movement although the wear rate remains constant. The findings underscore the importance of analyzing different parameters to understand the friction and wear properties of additively manufactured SS316L.

Keywords:
Laser powder bed fusion, Additive manufacturing, SS316L, Wear

1 INTRODUCTION

Additive Manufacturing (AM) particularly LPBF offers many applications optimized material usage and increased design workflows when compared to traditional manufacturing methodologies [Liu 2021]. SS316L esteemed for its austenitic properties and corrosion resistance plays an essential role in the aerospace, medical and chemical industries with LPBF facilitating improved accuracy in fabrication [DebRoy 2018]. Due to its austenitic characteristics and resistance to corrosion SS316L is essential in the aerospace, medical, and chemical sectors, with the LPBF technique increasing its application through remarkable in fabrication [Megahed 2016]. A focused laser beam of elevated intensity is directed toward the surface of the powder bed methodically melting and mixing the powder particles in stability with the parameters outlined in the digital model [Kempen 2011]. AM significantly reduces lead times by clearing out the need for manual tooling and setups. According to the findings of [Kruth 1998]. This plays a crucial role in allowing components to be fabricated within 24 hours a feat that is difficult to achieve with traditional machining methods. AM not only improves design flexibility but also increases operational efficiency particularly in the area of producing complex and personalized components. The layer-by-layer fabrication methodology allows the combination of internal characteristics such as mediums and lattice formations therefore improving the operational efficiency and utility of the produced components. Furthermore, the removal of tooling or preparatory procedures significantly accelerates production timelines when compared with conventional manufacturing techniques. LPBF is a highly effective technique for fabricating SS316L, offering improved material utilization, uninterrupted shaping, and the ability to create intricate geometries, aligning with [Dharmalingam 2022] findings on Direct Metal Laser Sintering (DMLS). Moreover, the resultant rough surface texture fails to align with the rigorous standards directed by aerospace and biomedical sectors, thereby requiring subsequent treatment processes to improve the surface characteristics of components produced by LPBF.

Although SS316L is extensively employed, its wear characteristics at elevated temperatures have not been thoroughly investigated, indicating a considerable deficiency in understanding, particularly regarding prospective applications within the automotive industry [Hao 2009]). The research gap centers on the limited understanding of high temperature wear behavior of SS316L produced through LPBF. Despite advances in AM techniques, studies focus mainly on mechanical properties, leaving wear resistance under elevated temperatures inadequately explored, as highlighted by [Gadalińska 2021]. This study identifies a significant gap in the literature, specifically related to the limited exploration of high-temperature wear resistance of SS316L components produced via LPBF. While mechanical properties have been well-documented, the impact of elevated thermal conditions on wear behavior has not been adequately addressed. Investigations into the tribological characteristics of SS316L fabricated by SLM indicate that diminished laser power correlates with decreased hardness and elevated wear rates, while increased scanning velocities contribute to improved wear resistance through

microstructural improvement. These empirical findings align with the statements posited by [Alphonse 2023] in their research, which explains the influence of process parameters on wear behavior and demonstrates that the optimization of these parameters can significantly enhance material performance and durability.

[Lei 2021] study shows that post-process heat treatments, including annealing and solution treatment, can improve wear performance by reducing residual stresses and facilitating beneficial microstructural changes. The results support the idea that optimizing build direction and laser power density is essential for improving the wear resistance and tribological characteristics of components made from SS316L using SLM. The study also found that higher laser energy density reduces porosity in SS316L which as a result improves its wear resistance. [Shanmuganathan 2023]. The influence of diverse post-processing methodologies including shot peening and surface polishing on the abrasion characteristics of SS316L produced via LPBF technology is analyzed [Walczak 2021] It was found that surface treatments significantly reduced the wear rate by improving surface quality and reducing microstructural flaws. [Gong 2014] research on fabricating Ti-6Al-4V components using AM shows that defects are strongly affected by changes in processing parameters which impact material performance under different conditions. Similarly, the heightened thermal conditions observed in selective laser melting (SLM) of SS316L contribute to an amplification of wear due to the formation of oxide layers thereby underscoring the imperative need for the refinement of process parameters or the application of protective treatments to improve wear resistance in environments characterized by elevated thermal conditions.

The objective of this study is to rigorously evaluate the tribological performance of SS316L alloy produced via LPBF under elevated thermal conditions, specifically between 150°C and 250°C. By addressing the previously unexplored wear behavior under these conditions, this research aims to bridge the existing literature gap and provide valuable insights into the suitability of LPBF-fabricated SS316L components for high-temperature, wear-resistant applications. Pin-on-disc tests reveal its applicability in high-temperature, wear-resistant industries.

2 MATERIALS AND METHODS

The SS316L pins were fabricated utilizing the LPBF technique with meticulous optimization of the process parameters to achieve higher quality. The chemical composition of the SS316L powder is shown in Tab. 1.

Tab. 1: Chemical composition of the SS316L.

Elements	Cr	Ni	Mo	C	N	Mn	Cu	P	S	Si	N	Fe
Wt. %	17.12	11	2.4	0.03	0.10	0.5	0.1	0.4	0.03	0.5	0.06	Bal.

The optimized LPBF parameters for fabricating high-quality SS316L pins (1.3 m/s scan velocity, 370 W power, 90 µm hatch spacing, 30 µm layer thickness) ensured precision and structural integrity. After fabrication, the pins (10 mm diameter, 30 mm length) underwent extensive microstructural analysis using optical microscopy, SEM, EDX, and EBSD techniques. Electro-polishing at -40°C with 11 V was performed for EBSD. These methods examined grain growth, texture orientation, and elemental composition, both before and after wear testing, offering critical insights into SS316L's microstructural properties and performance under high-temperature conditions.

2.1 Experimental Procedures and Sample Preparation for EBSD Analysis

High-temperature wear characteristics of the SS316L alloy fabricated through LPBF techniques were carefully evaluated utilizing a pin-on-disc tribometer. SS316L pins characterized by diameter of 10 mm and length of 30 mm were subjected to tribological testing against a titanium disc with hardness of 150 HV at elevated temperatures of 150°C and 250°C applied load of 5N and rotational speed of 300 rpm and testing duration of 30 minutes under conditions of dry sliding. The experimental investigations were performed in triplicate and resulting mean values together with their standard variations were calculated to increase the accuracy of the results. The assessment of wear rate and COF performed producing essential insights into the wear resistance and operational performance of SS316L under conditions of elevated temperature. In Electron Backscatter Diffraction (EBSD) analysis SS316L pins identical in dimensions to previously described and produced with optimized parameters of LPBF underwent a standardized metallographic preparation process. The electro-polishing procedure conducted at temperature of -40°C with a voltage application of 11 V in a solvent comprising 20% perchloric acid and 80% ethyl alcohol aimed to achieving a polished surface that facilitates accurate EBSD analysis. After that the samples were examined utilizing FEI Nova 450 HV SEM outfitted with the TSL-OIM EBSD package thereby providing crucial insights into the phenomena of grain growth texture orientation and the crystallographic coordination essential to the SS316L alloy.

2.2 Experimental Setup for Wear Testing

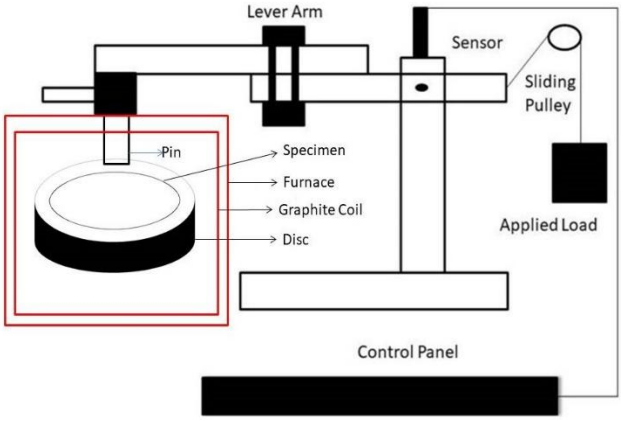

Fig. 1: Line sketch of pin – on - disc.

Wear tests were conducted using a DUCOM pin-on-disc tribometer (model TR-20-M-106) under dry sliding conditions with a titanium disc (150 HV hardness, 30 mm diameter, 10 mm thickness). Experimental were performed over a period of 30 minutes at thermal conditions of 150°C and 250°C with each experimental trial being replicated thrice to increase accuracy. Average values standard deviations were computed to determine the reliability of the

results. The tribological performance examined through the measurement of the wear volume thereby explaining the interactions occurring between the SS316L specimen and the titanium disc.

3 RESULTS AND DISCUSSION

3.1 Microscopic Analysis

Tribological evaluations conducted at 150°C and 250°C provided significant insights into the high-temperature wear properties of SS316L alloy produced through LPBF. The wear rate determined through the worn volume, applied load and sliding distance exhibited consistency across both thermal conditions indicating homogeneous wear mechanism. This stability is linked to the development of a protective oxide layer on the surfaces of the samples which direct metal-to-metal interaction and mitigates material. [Sun 2016] this investigation supports the earlier noted findings underscoring that the parameters of the LPBF process including laser power and scanning velocity significantly affect the microstructural characteristics and mechanical properties thereby supporting the development of oxide layers that wear stability at elevated thermal conditions ultimately increasing the performance of the alloy in environments.

The COF exhibited an increase from 150°C to 250°C attributable to the development of oxide films which despite mitigating wear resulted in an elevation of surface roughness and adhesion. The assessment of wear rate and COF conducted through the analysis of wear volume and track dimensions utilizing a three-dimensional profilometer. Subsequently the wear rate and COF were determined through the application of the relevant mathematical equations:

$$\text{Wear rate} = \frac{Worn\ volume}{Applied\ load\ x\ sliding\ distance} \quad (1)$$

$$\text{Coefficient of friction}, \mu = \frac{F}{N} \quad (2)$$

Here F indicate Frictional force and N is normal applied load in Newton respectively.

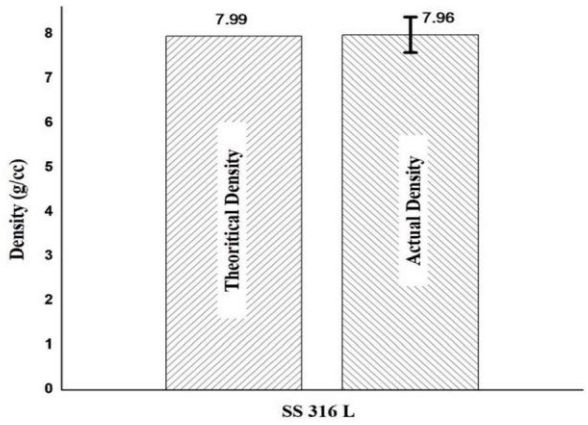

Fig. 2: Density analysis of theoretical and actual density.

Fig. 2 compares the theoretical and actual densities of the material to assess its quality. Theoretical density assumes perfect packing, while actual density reflects real material properties, including defects like pores and cracks. A significant difference between them, especially a lower actual density, indicates higher porosity, which can negatively affect mechanical performance. This comparison helps evaluate the manufacturing process and material suitability. Spierings et al. highlight the importance of precise density measurements, such as the Archimedes method, for evaluating additive manufacturing components, reinforcing the value of comparing theoretical and actual densities to assess porosity and material integrity [Spierings 2011].

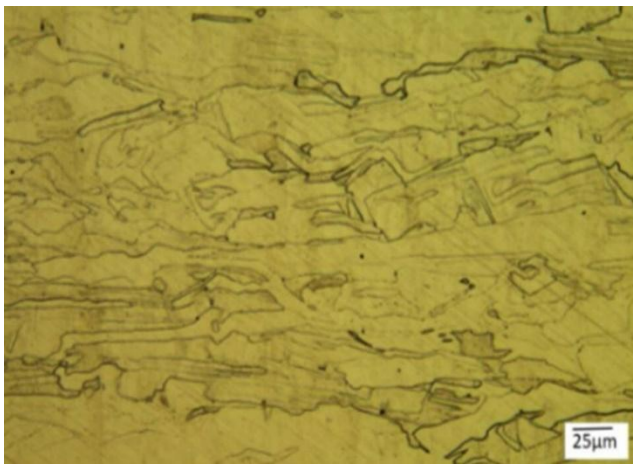

Fig. 3: Optical micrograph of SS316L before wear test.

Fig. 3 displays the microstructural features of SS316L fabricated through LPBF, showing minimal porosity and high-quality components. Spherical structures formed during solidification indicate a broad melt pool due to the laser's intense heat. The horizontal cross-section reveals scan tracks and partially fused melt pools. Study supports these findings, emphasizing how LPBF's solidification process creates melt pools, scan tracks, and reduced porosity, critical for producing high-density components with well-defined microstructures, reinforcing the effectiveness of LPBF in achieving superior material quality [Debroy 2017].

3.2 Wear Performance

The investigation into the wear performance of SS316L alloy produced by LPBF at 150°C and 250°C revealed key insights. The wear rate across both temperature conditions indicating uniform wear resistance and wear mechanism. This observed stability can be connected to the development of a protective oxide layer on the substrate which metallic interactions and mitigates material. However, the COF demonstrated an increase at elevated temperatures on the surface due to the formation of oxide films on the surface which subsequently amplified surface roughness and adhesive forces. [Bahshwan 2020] the findings presented are verified with particular emphasis placed on the significance of microstructural attributes of LPBF components in wear mechanisms as well as the implications of oxidation on wear rate stability and the COF under elevated temperature conditions.

Microstructural examination conducted via SEM and EEDX corroborated the presence of continuous and dense oxide films on the worn surfaces of SS316L with these films exhibiting greater prominence at 250°C. EDX analysis indicated that oxidation transpired during wear testing which subsequently increased wear resistance while simultaneously elevating friction levels. The phenomenon of oxidative wear observable at both temperature conditions characterized by the oxide layer functioning as a self-lubricating barrier which mitigated wear yet resulted in an increase in friction. Adhesive wear was more prominent at 250°C, where the elevated COF indicated stronger adhesive forces. [Shin 2021] research supports these findings, demonstrating that oxidation forms protective layers, which influence wear resistance and friction, with thicker oxide films and higher friction at elevated

temperatures. Before wear tests, the SS316L samples exhibited a compact microstructure with evenly distributed alloying elements and minimal porosity, highlighting the precision of the LPBF process. Post-test analysis revealed protective oxide layers, preserving structural integrity at high temperatures. These findings make LPBF-produced SS316L alloy suitable for high-temperature, wear-resistant applications in industries such as automotive and aerospace. However, for scenarios requiring minimal friction, post-processing techniques may be necessary to refine surface finish. The high-temperature wear behavior is marked by a stable wear rate due to oxide layer formation, which also increases friction.

3.3 Volumetric Wear Loss Analysis

To correlate the explanation provided with Fig. 4, which shows the volumetric wear loss for SS316L over varying sliding distances, we can align specific parts of the description with the graph. Initially, the text mentions that the wear rate is significantly heightened at the beginning of the test due to surface roughness, which is represented by an acute incline on the graph. This steep initial increase corresponds to the rapid material wear caused by the rough contact surfaces. As the test progresses, the wear rate becomes more stable, and the graph reflects this with a gentler slope, indicating a more uniform and steady wear rate.

As the sliding distance increases, the overall volumetric wear loss continues to grow, as shown by the upward trend in the curve. This demonstrates how wear loss accumulates over time with extended sliding distances (Tab. 2). Additionally, the explanation makes a comparison with the findings of [Alotaibi 2014] who observed a similar pattern of wear behavior, where an initially high wear rate due to surface roughness eventually stabilizes, transitioning to a steady-state wear phase. This overall trend—from sharp initial wear to stabilization—is consistent with both the experimental data depicted in Fig. 4 the graph captures the evolution of wear performance, correlating well with the description in the text.

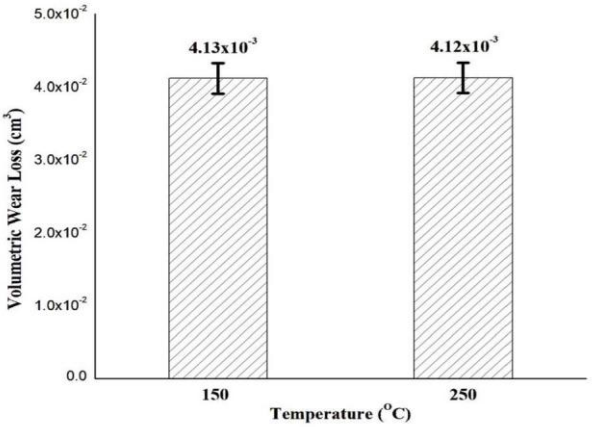

Fig. 4: Volumetric wear loss for SS316L for varying sliding distances.

Tab. 2: Wear test parameters for 5N Load at 150 °C and 250 °C temperature.

Sl. No.	Test load (N)	Sliding distance (m/s)	Sliding Velocity (m/s)	Time (Min)	Track Radius (mm)
1	5	2261.9	1.3	30	40
2	5	2261.9	1.3	30	40

3.4 After Wear Test SEM & EDX Results

The wear experiments in this study focused on examining the dry contact wear behavior of LPBF SS316L samples under dry sliding conditions.

Fig. 5a shows an SEM image of a worn SS316L sample under a 5N load at 150°C and 300 rpm, revealing wear tracks, debris, and surface irregularities. These features help identify wear mechanisms, such as abrasive, adhesive wear, or tribo-oxidation. Fig. 5b highlights a different region of the same sample, enabling comparison and identification of any discrepancies in wear patterns. Fig. 5c depicts a specimen under similar conditions, providing further insights into wear mechanisms, while Fig. 5d compares worn samples under varying conditions. [Farias 2007] emphasized that applied load and tangential velocity significantly influence wear mechanisms, surface roughness, and debris morphology, consistent with these SEM images showing how test parameters impact SS316L's wear behavior and surface morphology.

Fig. 6 shows EDX mapping of a worn surface subjected to 5N load, 300 rpm, and 150°C. Elemental maps for Fe, Cr, Ni, and O reveal wear characteristics. High Fe intensity suggests its dominance, while Cr and Ni indicate oxide formation. Uniform distribution implies even wear; clustering indicates localized wear or debris.

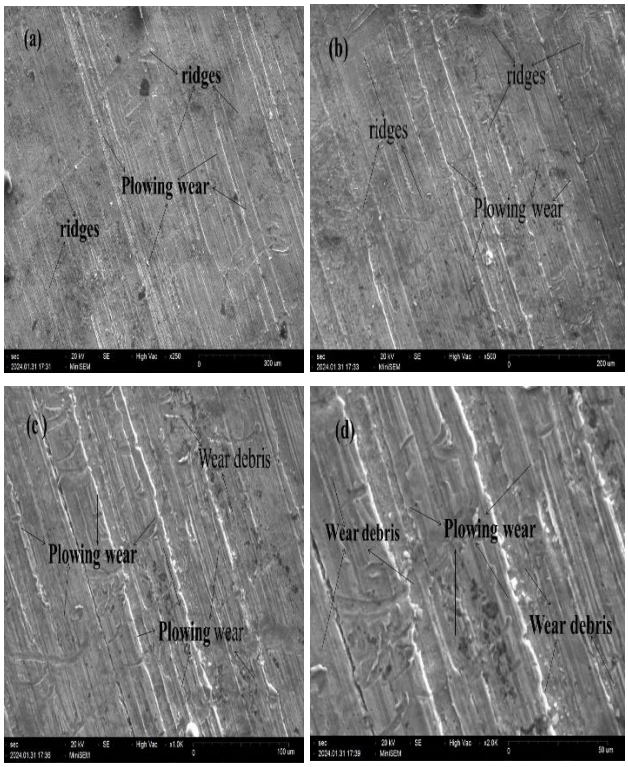

Fig. 5: SEM images of SS316L alloy after wear test at 5N load, 150°C and 300 rpm: (a) Wear surface morphology; (b)

Micro-crack formation; (c) Surface oxidation effects; (d) Evidence of abrasive wear.

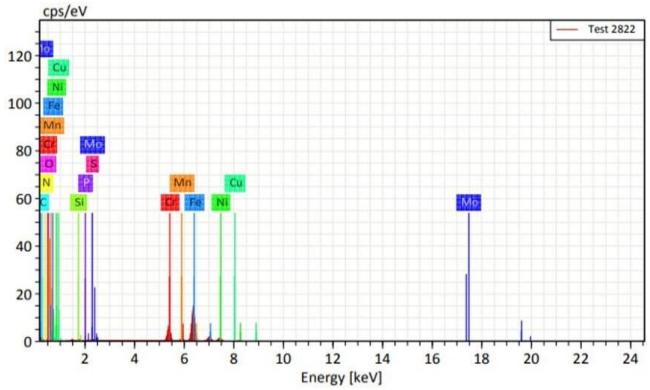

Fig. 6. EDX maps of the worn surface at 5N and speed 300 rpm at 150 temperatures.

Fig. 7a shows the surface morphology of a worn SS316L specimen at 250°C, highlighting wear tracks, debris, and surface features that indicate abrasive, adhesive wear, and tribo-oxidation. Fig. 7b reveals a different region of the same specimen, allowing comparison of wear patterns. Fig. 7c offers a magnified view, enabling detailed examination of microstructural changes, surface roughness, and wear debris morphology. Fig. 7d compares specimens under varying conditions, offering insights into the effects of temperature, load, and speed on SS316L wear behavior. [Lan 2021] findings align with these SEM images, showing that temperature and material composition influence oxidative and adhesive wear, emphasizing the importance of surface morphology in understanding wear mechanisms under different conditions.

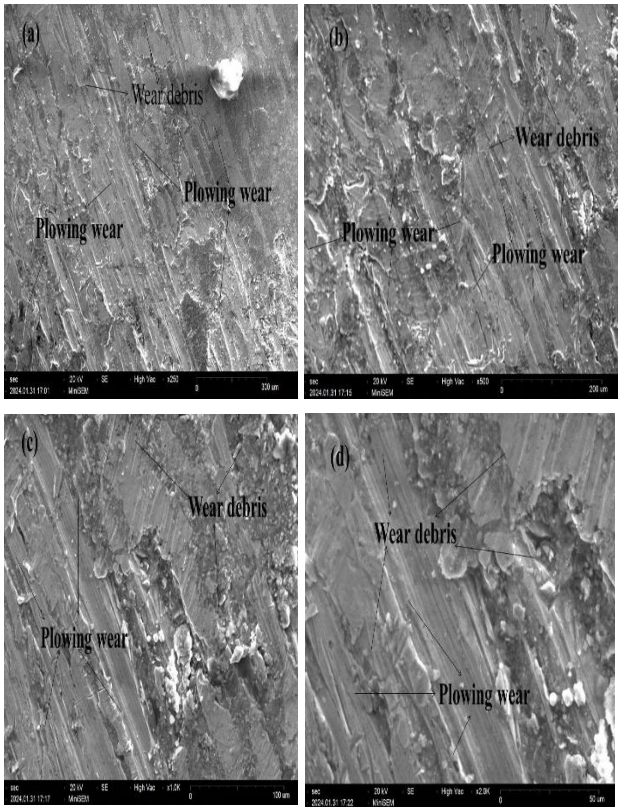

Fig. 7: SEM images of SS316L alloy after wear test at 5N load, 250°C and 300 rpm: (a) Wear surface morphology; (b) High magnification of wear tracks; (c) Oxide layer formation; (d) Localized wear region with adhesive wear.

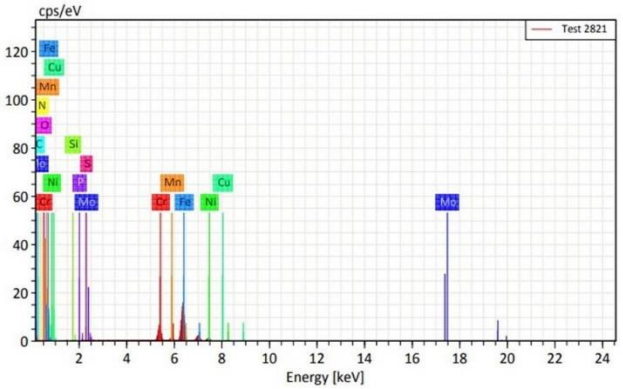

Fig. 8: EDX maps of the worn surface at 5N and speed 300 rpm at 250 temperatures.

Fig. 8 displays EDX maps of the worn SS316L surface under 5N load, 300 rpm, and 250°C, showing the distribution of elements like Fe, Cr, and Ni. Analysing these maps reveals variations in elemental composition, indicating wear mechanisms, oxide formation, and potential segregation or depletion caused by wear processes.

3.5 EBSD Analysis

EBSD is a microstructural-crystallographic technique used to examine the crystallographic orientation of materials. It's typically used in conjunction with a SEM.

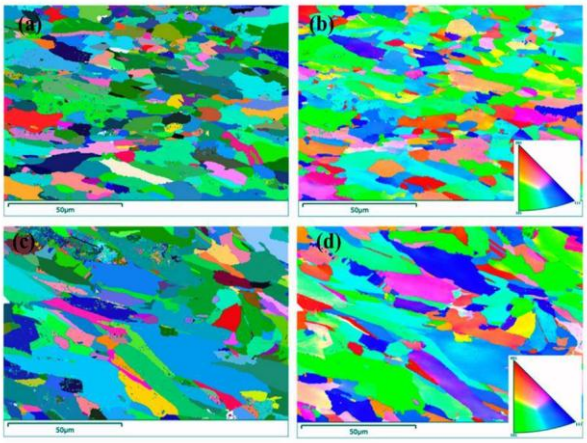

Fig. 9: (a-b) before and after (c-d) wear of SS316L: (a) Grain boundary (GB), (b) inverse pole figure (IPF).

Fig. 9: (a-b) before and after (c-d) wear of SS316L: (a) Grain boundary (GB), (b) inverse pole figure (IPF).

(a) Grain Boundary (GB) before wear: The microstructure of SS316L is depicted, with colours representing different grain orientations based on the Inverse Pole Figure (IPF) map. Grain boundaries, marked by colour changes, affect the material's strength, ductility, and corrosion resistance.

(b) Inverse Pole Figure (IPF) before wear: This color-coded orientation map illustrates the crystallographic arrangement of grains in SS316L, where specific colours correspond to crystal directions, providing insight into material texture.

(c) Grain Boundary (GB) after wear: post-wear microstructural changes, including variations in grain size, morphology, and orientation, suggest wear-induced deformation, grain refinement, and increased dislocation density.

(d) Inverse Pole Figure (IPF) after wear: post-wear map shows how grain orientations have shifted due to mechanical stress.

Comparing pre- and post-wear maps provides insights into wear mechanisms and aids in improving SS316L's wear resistance through microstructure optimization.

4 CONCLUSIONS

- Wear tests on SS316L samples manufactured by the laser powder bed fusion (LPBF) process were performed using a pin-on-disc tribometer.
- Results demonstrated that both micro- and macro-surface properties of the as-built LPBF specimens significantly affect their wear performance.
- Experiments were conducted at thermal conditions ranging from 150°C to 250°C, with a sliding velocity of 300 rpm and a load of 5N.
- The wear behavior of SS316L pins produced via LPBF was influenced by factors such as applied load, Testing, Sliding speed.
- In the temperature spectrum from 150°C to 250°C an elevation in the coefficient of friction (COF) was observed and the wear rate exhibited consistent stability.
- This study emphasizes the importance of considering various wear conditions to enhance the wear resistance of LPBF components.
- Evaluating the wear characteristics of SS316L pins made through LPBF provides insights into their performance under different sliding conditions.
- These insights aid in the development of more durable and effective LPBF components for challenging wear environments.

ACKNOWLEDGMENTS

This article was co-funded by the European Union under the REFRESH – Research Excellence For REgion Sustainability and High-tech Industries project number CZ.10.03.01/00/22_003/0000048 via the Operational Programme Just Transition and has been done in connection with project Students Grant Competition SP2024/087 "Specific Research of Sustainable Manufacturing Technologies“ financed by the Ministry of Education, Youth and Sports and Faculty of Mechanical Engineering VŠB-TUO.

REFERENCES

[Alotaibi 2014] Alotaibi, J. G., Yousif, B. F., & Yusaf, T. F. (2014). Wear behaviour and mechanism of different metals sliding against stainless steel counterface. Proceedings of the Institution of Mechanical Engineers, Part J: Journal of Engineering Tribology, 228(6), 692–704. https://doi.org/10.1177/1350650114527072

[Alphonse 2023] Alphonse, M., Murali, A. P., Salunkhe, S., Gawade, S. R., Naveen Kumar, B. V. S. G., Nasr, E. A., & Kamrani, A. (2023). Analysis of Wear Using the Taguchi Method in TiSiNOS-Coated and Uncoated H13 Tool Steel. Coatings, 13(10). https://doi.org/10.3390/coatings13101781

[Bahshwan 2020] Bahshwan, M., Myant, C. W., Reddyhoff, T., & Pham, M. S. (2020). The role of microstructure on wear mechanisms and anisotropy of additively manufactured 316L stainless steel in dry sliding. Materials and Design, 196. https://doi.org/10.1016/j.matdes.2020.109076

[Debroy 2017] Debroy, T., Wei, H. L., Zuback, J. S., Mukherjee, T., Elmer, J. W., Milewski, J. O., Beese, A. M., Wilson-Heid, A., De, A., & Zhang, W. (2017). Additive manufacturing of metallic components – Process, structure and properties. https://www.sciencedirect.com/science/article/pii/S0079642517301172

[Debroy 2018] DebRoy, T., Wei, H. L., Zuback, J. S., Mukherjee, T., Elmer, J. W., Milewski, J. O., Beese, A. M., Wilson-Heid, A., De, A., & Zhang, W. (2018). Additive manufacturing of metallic components – Process, structure and properties. In Progress in Materials Science (Vol. 92, pp. 112–224). Elsevier Ltd. https://doi.org/10.1016/j.pmatsci.2017.10.001

[Dharmalingam 2022] Dharmalingam, G., Baskar, R., Arun Prasad, M., & Salunkhe, S. (2022). Development of microstructure - processing correlations of Inconel718 through additive manufacturing. Materials Today: Proceedings, 68, 1891–1897. https://doi.org/10.1016/j.matpr.2022.08.062

[Farisa 2007] Farias, M. C. M., Souza, R. M., Sinatora, A., & Tanaka, D. K. (2007). The influence of applied load, sliding velocity and martensitic transformation on the unlubricated sliding wear of austenitic stainless steels. Wear, 263(1-6 SPEC. ISS.), 773–781. https://doi.org/10.1016/j.wear.2006.12.017

[Gadalinska 2021] Gadalińska, E., Pawliszak, Ł., & Moneta, G. (2021). Laser Powder Bed Fusion and Selective Laser Melted Components Investigated with Highly Penetrating Radiation. Fatigue of Aircraft Structures, 2021(13), 81–98. https://doi.org/10.2478/fas-2021-0008

[Gong 2014] Gong, H., Rafi, K., Gu, H., Starr, T., & Stucker, B. (2014). Analysis of defect generation in Ti-6Al-4V parts made using powder bed fusion additive manufacturing processes. Additive Manufacturing, 1, 87–98. https://doi.org/10.1016/j.addma.2014.08.002

[Hao 2009] Hao, L., Dadbakhsh, S., Seaman, O., & Felstead, M. (2009). Selective laser melting of a stainless steel and hydroxyapatite composite for load-bearing implant development. Journal of Materials Processing Technology, 209(17), 5793–5801. https://doi.org/10.1016/j.jmatprotec.2009.06.012

[Kempen 2011] Kempen, K., Thijs, L., Yasa, E., Badrossamay, M., Verheecke°, W., & Kruth, J.-P. (n.d.). PROCESS OPTIMIZATION AND MICROSTRUCTURAL ANALYSIS FOR SELECTIVE LASER MELTING OF AlSi10Mg.

[Kruth 1998] Kruth, J. P., Leu, M. C., & Nakagawa, T. (1998). Progress in additive manufacturing and rapid prototyping. CIRP Annals - Manufacturing Technology, 47(2), 525–540. https://doi.org/10.1016/S0007-8506(07)63240-5

[Lan 2021] Lan, L. W., Yang, H. J., Guo, R. P., Wang, X. J., Zhang, M., Liaw, P. K., & Qiao, J. W. (2021). High-temperature sliding wear behavior of nitrided Ni45(CoCrFe)40(AlTi)15 high-entropy alloys. Materials Chemistry and Physics, 270. https://doi.org/10.1016/j.matchemphys.2021.124800

[Lei 2021] Lei, J., Ge, Y., Liu, T., & Wei, Z. (2021). Effects of Heat Treatment on the Microstructure and Mechanical Properties of Selective Laser Melting 316L Stainless Steel. Shock and Vibration, 2021. https://doi.org/10.1155/2021/6547213

[Liu 2021] Liu, G., Zhang, X., Chen, X., He, Y., Cheng, L., Huo, M., Yin, J., Hao, F., Chen, S., Wang, P., Yi, S., Wan, L., Mao, Z., Chen, Z., Wang, X., Cao, Z., & Lu, J. (2021). Additive manufacturing of structural materials. In Materials

Science and Engineering R: Reports (Vol. 145). Elsevier Ltd. https://doi.org/10.1016/j.mser.2020.100596

[Megahed 2016] Megahed, M., Mindt, H. W., N'Dri, N., Duan, H., & Desmaison, O. (2016). Metal additive-manufacturing process and residual stress modeling. In Integrating Materials and Manufacturing Innovation (Vol. 5, Issue 1, pp. 61–93). Springer Science and Business Media Deutschland GmbH. https://doi.org/10.1186/s40192-016-0047-2

[Shanmuganathan 2023] Shanmuganathan, P. K., Purushothaman, D. B., & Ponnusamy, M. (2023). Effect of High Laser Energy Density on Selective Laser Melted 316L Stainless Steel: Analysis on Metallurgical and Mechanical Properties and Comparison with Wrought 316L Stainless Steel. 3D Printing and Additive Manufacturing, 10(3), 383–392. https://doi.org/10.1089/3dp.2021.0061

[Shin 2021] Shin, W. S., Son, B., Song, W., Sohn, H., Jang, H., Kim, Y. J., & Park, C. (2021). Heat treatment effect on the microstructure, mechanical properties, and wear behaviors of stainless steel 316L prepared via selective laser melting. Materials Science and Engineering: A, 806(December 2020), 140805. https://doi.org/10.1016/j.msea.2021.140805

[Spierings 2011] Spierings, A. B., Schneider, M., & Eggenberger, R. (2011). Comparison of density measurement techniques for additive manufactured metallic parts. Rapid Prototyping Journal, 17(5), 380–386. https://doi.org/10.1108/13552541111156504

[Sun 2016] Sun, Z., Tan, X., Tor, S. B., & Yeong, W. Y. (2016). Selective laser melting of stainless steel 316L with low porosity and high build rates. Materials and Design, 104, 197–204. https://doi.org/10.1016/j.matdes.2016.05.035

[Walczak 2012] Walczak, M., & Szala, M. (2021). Effect of shot peening on the surface properties, corrosion and wear performance of 17-4PH steel produced by DMLS additive manufacturing. Archives of Civil and Mechanical Engineering, 21(4). https://doi.org/10.1007/s43452-021-00306-3